Applied Physics Letters

RESEARCH ARTICLE | JULY 15 2026

Structural control of molybdenum oxide by post-treatment processes

Makoto Kashiwagi ; Shota Chomei; Takehiko Yokomori; Yuki Oguchi; Yuzo Shigesato

Appl. Phys. Lett. 129, 021909 (2026)
https://doi.org/10.1063/5.0331910

Applied Physics Letters ARTICLE pubs.aip.org/aip/apl

Structural control of molybdenum oxide by post-treatment processes

Cite as: Appl. Phys. Lett. **129**, 021909 (2026); doi: 10.1063/5.0331910
Submitted: 28 February 2026 · Accepted: 27 April 2026 ·
Published Online: 15 July 2026

Makoto Kashiwagi,[1,2,3] Shota Chomei,[1] Takehiko Yokomori,[4] Yuki Oguchi,[5] and Yuzo Shigesato[1,a)]

AFFILIATIONS

[1]Graduate School of Science and Engineering, Aoyama Gakuin University, Sagamihara, Kanagawa 252-5258, Japan
[2]Research Organization for Nano & Life Innovation, Waseda University, Shinjuku-ku, Tokyo 162-0041, Japan
[3]PRESTO, Japan Science and Technology Agency, Kawaguchi, Saitama 332-0012, Japan
[4]Technology & Engineering Department, Photon Global Business Unit, Ushio, Inc., Himeji, Hyogo 671-0224, Japan
[5]Center for Instrumental Analysis, College of Science and Engineering, Aoyama Gakuin University, Sagamihara 252-5258, Japan

[a)]**Author to whom correspondence should be addressed:** yuzo@chem.aoyama.ac.jp

ABSTRACT

To investigate the crystallization behavior and controllability of the crystal structure of MoO_3, we conducted crystallization of amorphous MoO_3 (a-MoO_3) and a structural phase transition of polycrystalline MoO_3 through post-treatment processes, such as thermal or flashlamp annealing, followed by the crystal structure analyses by x-ray diffraction. These results clarified the relationship between the activation energies of the crystallization of a-MoO_3 to α-MoO_3 or β-MoO_3, as well as the structural phase transition of β-MoO_3 to α-MoO_3. Additionally, we demonstrated the controllability of MoO_3 crystals using these processes.

Recently, electrochromic (EC) materials have attracted attention as optical materials.[1,2] Electrochromic displays using EC materials are expected to be the next-generation of displays because EC materials have features such as visibility in bright environments, high contrast, independence from viewing angle, and scalability. Additionally, EC materials are expected to be used in electrochromic dimming glass for energy-saving devices that control sunlight exposure. Tungsten oxide (WO_3) exhibits excellent EC properties, such as a fast response time, coloration efficiency, and a long lifetime. It is the most widely studied EC material.[3–13] Molybdenum oxide (MoO_3) is also an EC material that has attracted much attention.[14–19] Since Mo has a relatively small atomic size, MoO_3 is expected to exhibit superior ionic diffusion properties. Additionally, the electrochromic response of MoO_3 is characterized by stronger and more uniform light absorption in its colored state compared to WO3. Furthermore, MoO_3 shows high apparent coloration efficiency. This is because the optical absorption peak of molybdenum bronze is found closer to the sensitivity peak of the human eye.[16,20,21] However, a limited number of studies have reported on the electrochromism of MoO_3.[22] The complete coloration mechanism of MoO_3 is explained by the small polaron absorption model as well as WO_3.[11,17–19,23] In the small polaron absorption model, the absorption coefficient α is expressed by the following equation:[11,13]

$$\alpha(\hbar\omega) \propto \exp\left[\frac{-(\hbar\omega - \varepsilon - 4U)}{8U\hbar\omega_0}\right], \quad (1)$$

where $\hbar\omega$ is the energy of incident light, $\hbar\omega_0$ is the phonon energy, ε is the site-specific potential variation, and U is the polaron stabilization energy (PSE). The polaron stabilization energy depends heavily on the crystal structure. In the amorphous structure, the PSE should be large because the electron–phonon interactions are stronger due to the localization of electrons in the random potentials in disrupted periodicity. In contrast, in the crystal structure, the PSE becomes smaller in a crystal structure because the electron–phonon interaction decreases as electrons become delocalized with increasing crystallinity. Thus, as the crystallinity increases, the PSE decreases and the absorption peak shifts to lower energies. Thus, crystal structure strongly influences the optical absorption of EC materials. Controlling the crystallinity of EC materials is therefore important for their application in optical devices. MoO_3 has two stable crystal structures: the thermodynamically most stable structure α-MoO_3 and the metastable structure β-MoO_3.[17,23] These polymorphs and the amorphous state exhibit different behaviors regarding ion intercalation and structural stability. The α-MoO_3 phase has an orthorhombic layered structure composed of stacked bilayers of distorted MoO_6 octahedra. In each

bilayer, distorted MoO_6 octahedra are interconnected via edge sharing, whereas adjacent bilayers interact via van der Waals forces. The α-MoO_3 structure is the most extensively studied for electrochromic applications due to its high theoretical capacity and potential for high energy density.[16,20,21] The β-MoO_3 phase is a ReO_3-type structure with corner-shared octahedra that facilitates higher reaction potentials. Moreover, as mentioned above, increasing crystallinity modifies the PSE and optical response.[22] In contrast, a-MoO_3 has been shown to provide superior long-term cycling stability because it undergoes less structural change upon ion insertion.[22] It is therefore important to establish a method of controlling the crystal structure for application to devices since various material properties depend on the crystal structure, as mentioned above. In this study, we investigated the crystallization behavior of post-treated MoO_3 to reveal its crystallization mechanism and verify the controllability of its crystal structure through post-treatment processes. In this study, thermal and flashlamp annealing (FLA) were used for post-treatment.

In this study, the crystallization behavior of MoO_3 was investigated using a-MoO_3 and polycrystalline MoO_3 thin films deposited by reactive DC magnetron sputtering using a molybdenum (Mo) metal target and a mixture of Ar-O_2 gases. The MoO_3 thin films were deposited on a quartz glass. The O_2 flow rate during deposition was set to 40.0%, the total gas pressure was kept at 0.5 Pa, and the sputtering power was set to 100 W. To investigate the effect of the post-thermal treatment process on crystallization, the fabricated a-MoO_3 and polycrystalline MoO_3 thin films were treated by thermal annealing under atmospheric air. The a-MoO_3 thin films were post-thermal annealed from 180 to 500 °C, and the annealing time was set from 60 to 420 min. The polycrystalline MoO_3 thin films were post-thermal annealed from 250 to 400 °C for 60 min. Additionally, the fabricated a-MoO_3 and polycrystalline MoO_3 films were post-treated by flashlamp annealing (FLA). FLA enables photoreduction and photocrystallization by instantaneously irradiating the sample with intense light.[24–27] FLA is expected to be the post-treatment process for electrical devices due to its high processing speed and minimal thermal damage. The FLA device used in this study was manufactured by USHIO INC. and irradiates light with wavelengths ranging from ultraviolet to visible and near-infrared. The intensity of the irradiating light was controlled by adjusting the forward voltage to the capacitor. To investigate the effect of flashlamp irradiation on crystallization, the a-MoO_3 thin films were irradiated at intensities ranging from 70% to 140%, and the polycrystalline MoO_3 thin films were irradiated at 100%, 120%, and 140% intensity. Note that the light energy density in this experiment is about 3.5 J/cm^2 at 100%. The optical property of a-MoO3 and the spectrum of irradiated flashlamp are shown in the supplementary material (see Fig. S1 in the supplementary material). The crystallographic structure was analyzed by x-ray diffraction (XRD) with Cu Kα1 radiation at 40 kV and 20 mA (XRD-6000, Shimadzu) and Raman spectroscopy (in Via Reflex, RENISHAW). In the manuscript, only the ranges of the crystallographic analyses that most clearly show the crystallization behavior are presented; the full-range measurement results are provided in the Supplementary Material (see Figs. S2 through S6).

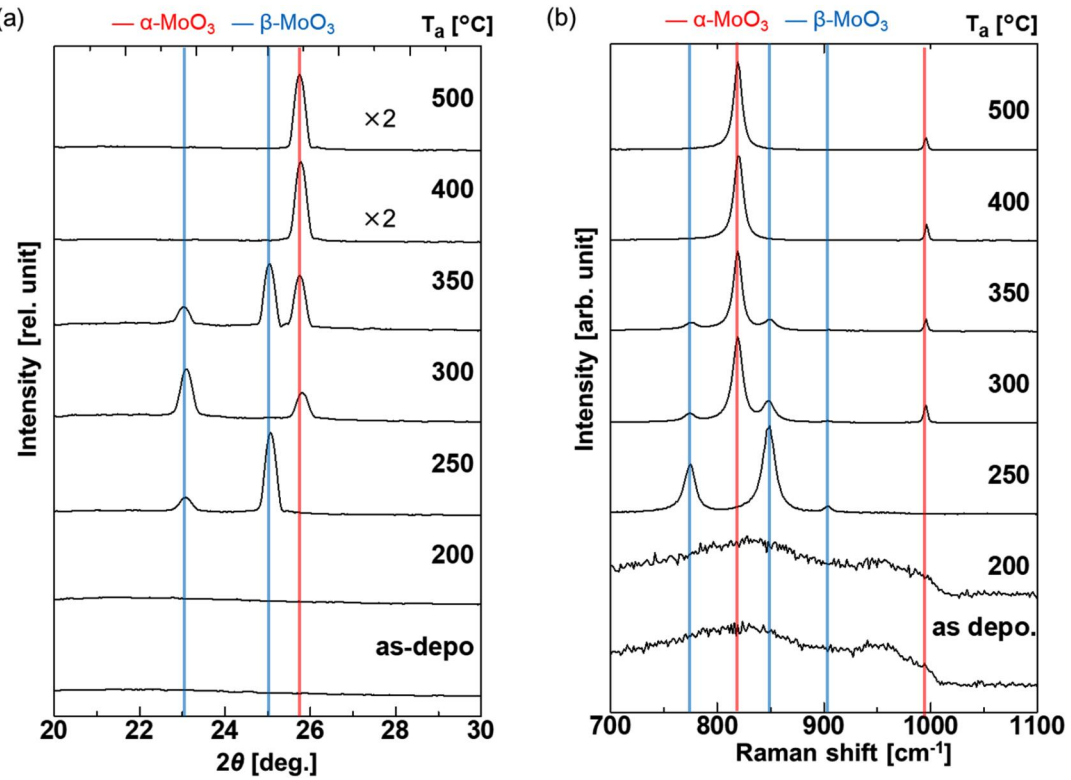

FIG. 1. XRD pattern and Raman spectra of the post-thermal annealed a-MoO_3 with annealing time of 60 min. The red lines show the peaks corresponding to α-MoO_3 and the blue lines show the peaks corresponding to β-MoO_3. (a) XRD pattern, (b) Raman spectra.

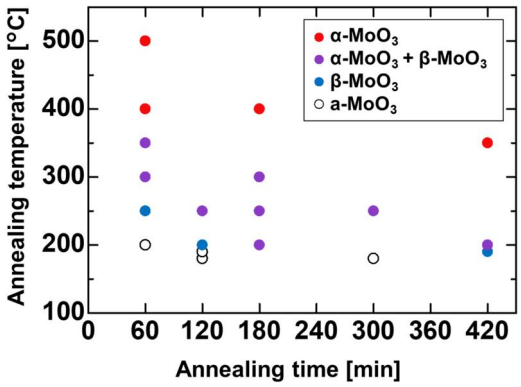

FIG. 2. Summary of the crystal state of the post-thermal annealed a-MoO_3. The open circle represents the a-MoO_3 structure, the blue circle represents the single-phase β-MoO_3 structure, the purple circle represents the mixed structure of α-MoO_3 and β-MoO_3, and the red circle represents the single-phase α-MoO_3 structure.

The structural change of the MoO_3 films upon post-thermal annealing is first presented. Figure 1 shows the XRD results and Raman spectra of a-MoO_3 samples that were thermally annealed for 60 min. These results show that the XRD and Raman spectroscopy results were in good agreement. Specifically, the XRD results of the sample annealed at 200 °C showed a halo pattern and the Raman spectrum of the sample annealed at 200 °C showed no peaks corresponding to the crystalline structure. The results of samples annealed at 250 °C showed only the peaks of β-MoO_3, and the results of samples annealed at 300 and 350 °C showed the peaks corresponding to α-MoO_3 and β-MoO_3. Only the peaks of α-MoO_3 were observed in the results of annealing temperatures above 400 °C. Note that the crystallization behavior is also analyzed using TEM observations and electron diffraction, and these results were in good agreement with the XRD results and Raman spectroscopy (see Figs. S7–S9 in the supplementary material). Figure 2 summarizes the crystal state of post-thermal annealed a-MoO_3. These results show that the crystal structure of α-MoO_3 does not change with post-thermal annealing below 190 °C. A single-phase β-MoO_3 structure was confirmed at an annealing temperature above 200 °C with a short annealing time of less than 120 min. A mixed structure of α-MoO_3 and β-MoO_3 was confirmed at an annealing temperature above 200 °C with a long annealing time. A single-phase β-MoO_3 structure was confirmed at an annealing temperature above 400 °C or at an annealing temperature above 350 °C with a long annealing time (more than 7 h). These results are consistent with the results of thermal treatment during deposition. That is, these results demonstrate that the activation energy for crystallization from a-MoO_3 to β-MoO_3 is lower than the activation energy for crystallization from a-MoO_3 to α-MoO_3. Figure 3 shows the XRD results for thermal annealed polycrystalline MoO_3 samples. Note that these results are from polycrystalline MoO_3 films deposited by heating the substrate at 250 and 350 °C. Figures 3(a) and 3(b) show the results of

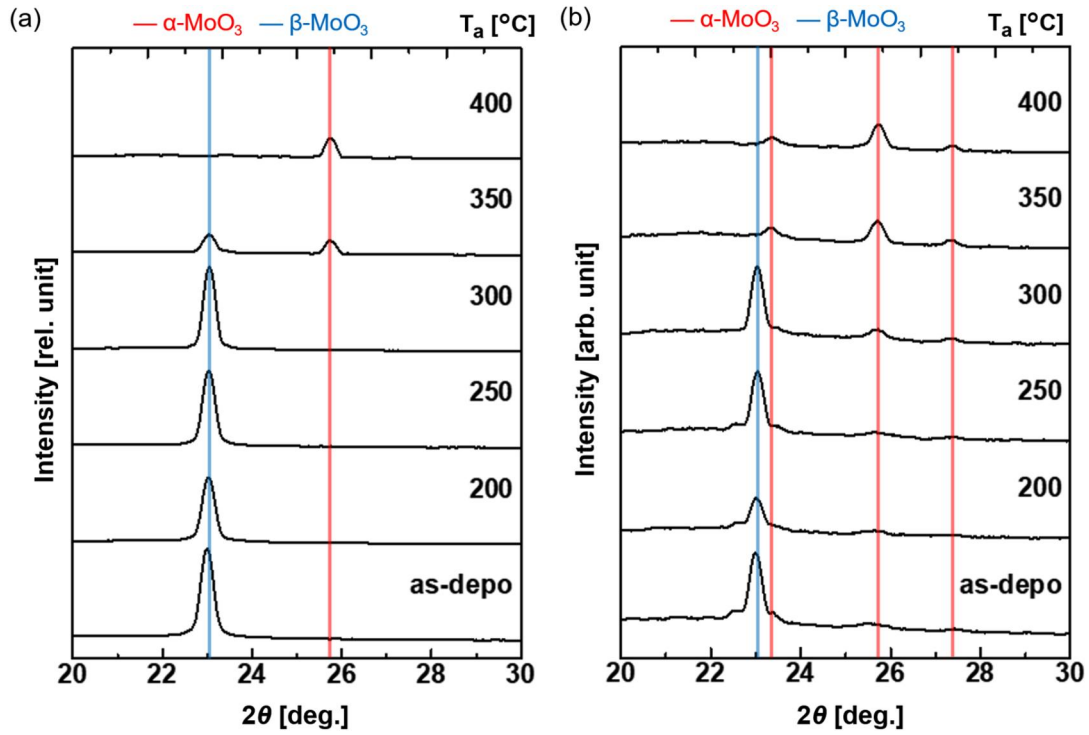

FIG. 3. XRD pattern of the post-thermal annealed polycrystalline MoO_3 with annealing time of 60 min. The red lines show the peaks corresponding to α MoO_3 and the blue-lines show the peaks corresponding to β-MoO_3. (a) The polycrystalline MoO_3 deposited with substrate heating at 250 °C. (b) The polycrystalline MoO_3 deposited with substrate heating at 350 °C.

post-thermal annealed polycrystalline MoO_3 deposited at 250 and 350 °C, respectively. The crystalline structure of the as-deposited MoO_3 deposited at 250 °C was a single-phase β-MoO_3 structure. The crystalline structure of the as-deposited MoO_3 deposited at 350 °C was a mixed structure of α-MoO_3 and β-MoO_3. As shown in Fig. 3(a), the β-MoO_3 crystal structure did not change at annealing temperatures below 300 °C. The α-MoO_3 structure appeared at an annealing temperature of 350 °C, and the α-MoO_3 single-phase structure was confirmed at an annealing temperature of 400 °C. As shown in Fig. 3(b), the mixed α-MoO_3 and β-MoO_3 crystal structures were almost unchanged by post-thermal annealing below 300 °C. Post-thermal annealing at 350 °C decreased the peaks corresponding to the β-MoO_3 structure and increased the peaks corresponding to the α-MoO_3 structure. In other words, the structural phase transition from β-MoO_3 to α-MoO_3 occurred by post-thermal annealing above 350 °C. According to the post-annealing results, the activation energy for crystallization from a-MoO_3 to β-MoO_3 was lower than the activation energy for crystallization from a-MoO_3 to α-MoO_3. Furthermore, crystallization from a-MoO_3 to α-MoO_3 occurred at an annealing temperature of 300 °C, while the structural phase transition from β-MoO_3 to α-MoO_3 occurred at an annealing temperature above 350 °C. These results reveal that the activation energy for the structural phase transition from β-MoO_3 to α-MoO_3 is higher than the one for crystallization from a-MoO_3 to α-MoO_3. The relationship between these activation energies can be summarized as follows:

$$E_a(a \rightarrow \beta) < E_a(a \rightarrow \alpha) < E_a(\beta \rightarrow \alpha), \tag{2}$$

where $E_a(a \rightarrow \beta)$, $E_a(a \rightarrow \alpha)$, and $E_a(\beta \rightarrow \alpha)$ are the activation energies of crystallization from a-MoO_3 to β-MoO_3, from a-MoO_3 to α-MoO_3, and the activation energy of structural phase transition from β-MoO_3 to α-MoO_3, respectively. The energy diagram showing the activation energies of crystallization and phase transitions is provided in the supplementary material (see Fig. S12 in the supplementary material).

Following the characterization of post-thermal annealed MoO_3, we now focus on the structural change induced by flash-lamp annealing (FLA). Figures 4 and 5 show the XRD results and Raman spectra for flashlamp annealed a-MoO_3 and polycrystalline β-MoO_3 samples. As shown in the results of a-MoO_3, the crystal structure of a-MoO_3 did not change when irradiated at 100% intensity. The structure of β-MoO_3 was confirmed by irradiation at 110% and 120% intensity, while the structure of α-MoO_3 was confirmed by irradiation at over 130% intensity. In the results of flashlamp annealed β-MoO_3, the structural phase transition from β-MoO_3 to α-MoO_3 was not confirmed even by irradiation at

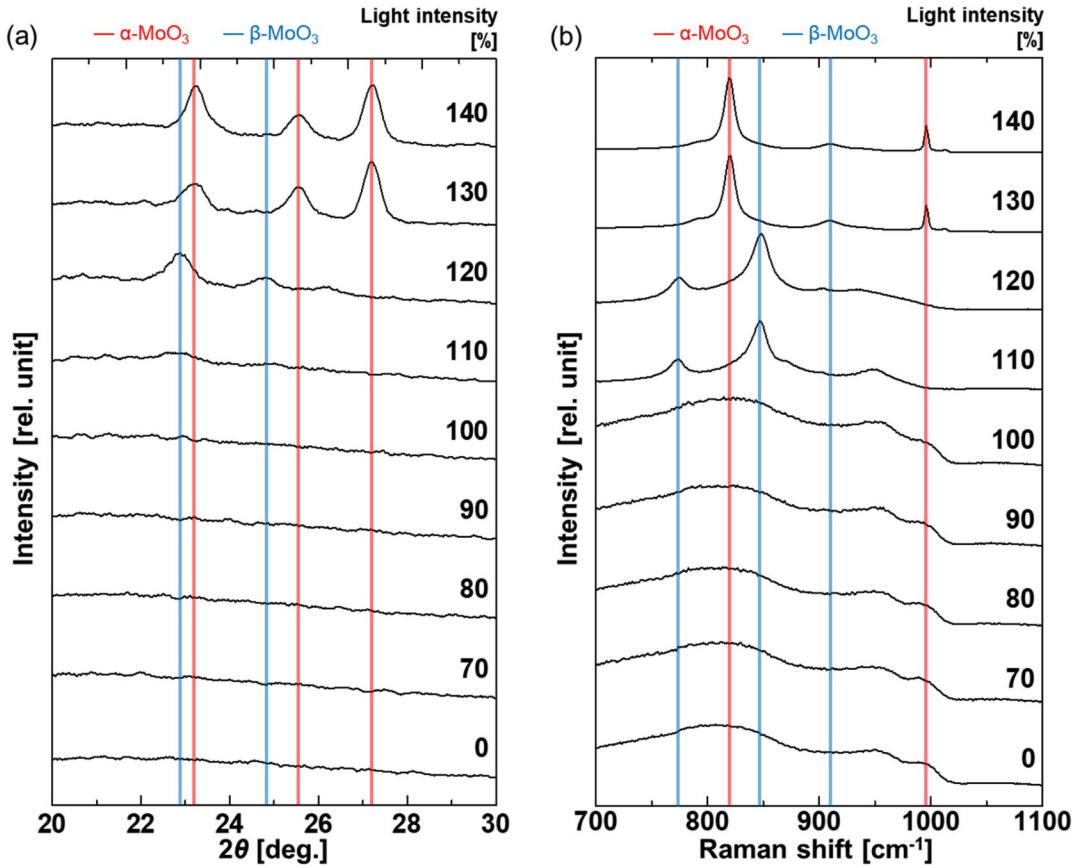

FIG. 4. XRD pattern and Raman spectra of the post-flashlamp annealed a-MoO_3 with irradiation time of 0.2 ms. The red lines show the peaks corresponding to α-MoO_3 and the blue lines show the peaks corresponding to β-MoO_3. (a) XRD pattern (2θ scan), (b) Raman spectra.

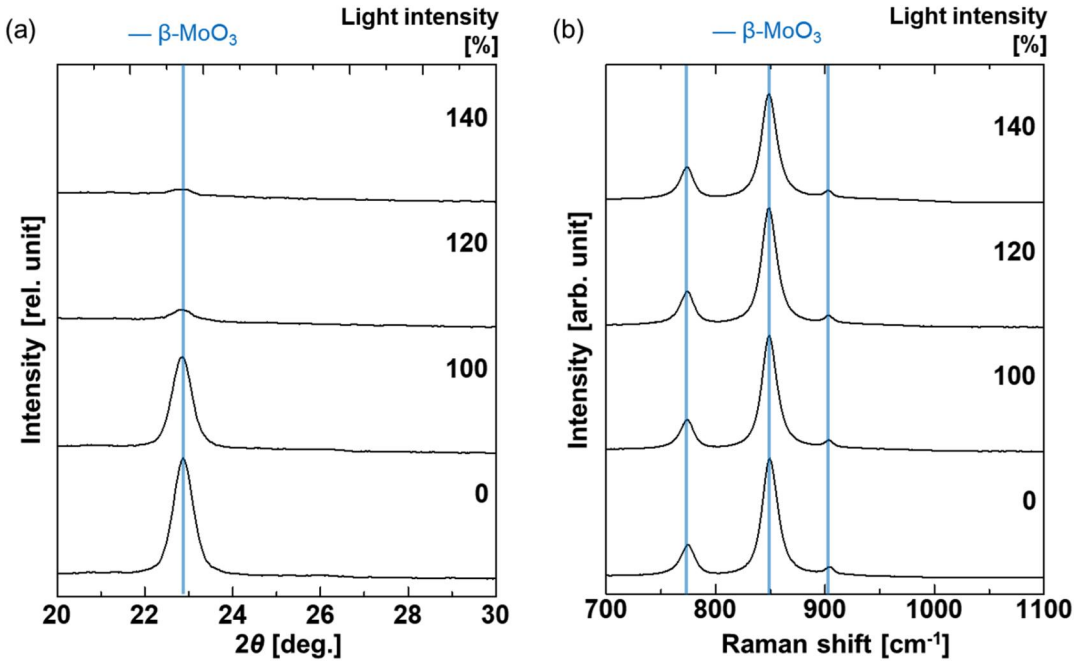

FIG. 5. XRD pattern and Raman spectra of the post-flashlamp annealed polycrystalline MoO_3 with irradiation time of 0.2 ms. The polycrystalline MoO_3 thin films were deposited with substrate heating at 250 °C. The red lines show the peaks corresponding to α-MoO_3 and the blue lines show the peaks corresponding to β-MoO_3. (a) XRD pattern (2θ scan), (b) Raman spectra.

140% intensity. These results indicate that a higher level of irradiation energy is necessary for the structural phase transition from β-MoO_3 to α-MoO_3. Note that the crystallization behavior is also analyzed using TEM observations and electron diffraction, and these results were in good agreement with the XRD results and Raman spectroscopy (see Figs. S10 and S11 in the supplementary material). These results are in good agreement with the results of thermal annealing: the crystallization energy from a-MoO_3 to α-MoO_3 is higher than the crystallization energy from a-MoO_3 to β-MoO_3, and the structural phase transition energy from β-MoO_3 to α-MoO_3 is even higher. To verify the effect of temperature increase by flashlamp irradiation on crystallization in FLA process, we irradiated the flashlamp with irradiation power of 110, 120, 130, 140% on a-MoO_3 cooled by liquid nitrogen. Figure 6 shows the XRD results of the cooled a-MoO_3 samples. The β-MoO_3 structure was confirmed with irradiation of 120% intensity, the α-MoO_3 structure was confirmed with irradiation of over 120% intensity, and the single-phase α-MoO_3 was confirmed with irradiation of over 130% intensity. These results are in close agreement with the results of FLA without cooling. Thus, we concluded that the temperature increase from flashlamp irradiation has a negligible effect on crystallization. Additionally, unlike the results of thermally annealed samples, the mixed structure of α-MoO_3 and β-MoO_3 did not appear in the results of flashlamp irradiation. We considered that the difference was due to the difference in energy supply time for each process. In the thermal annealing process, the temperature increases at a rate of 3–8 °C/min. Therefore, even at the temperature exceeds 250 °C, the temperature at which crystallization from amorphous MoO_3 to α-MoO_3 occurs, the MoO_3 thin film first passes through approximately 200 °C during the heating, where crystallization from amorphous MoO_3 to β-MoO_3 can occur. Furthermore, the β-MoO_3 cannot change into α-MoO_3 in the thermal annealing process below 350 °C. Consequently, the mixed structure of α-MoO_3 and β-MoO_3 appeared in the thermal annealing process. In contrast, in flashlamp annealing, the light irradiation time is only 0.2 milliseconds and delivers energy for a very short time compared to thermal annealing. In contrast, during photoirradiation at above 130% intensity, which provides sufficient energy for crystallization from amorphous MoO_3 to α-MoO_3, the films do not experience a lower-energy stage corresponding to irradiation below 120%, which induces crystallization from amorphous MoO_3 to β-MoO_3. Therefore, flashlamp annealing can be used to obtain a single-phase sample with only β-MoO_3 or α-MoO_3 structures.

In this study, we investigated the change in the crystal structure of MoO_3 using post-treatment processes such as thermal and flashlamp annealing. We clarified the crystallization mechanism of MoO_3 and explored the possibility of controlling its structure. The results of the post-treatment process revealed that the activation energy of crystallization from a-MoO_3 to α-MoO_3 is higher than that from a-MoO_3 to β-MoO_3, and the energy of structural phase transition from β-MoO_3 to α-MoO_3 is even higher. The relationship between the activation energies is shown in Eq. (2). Regarding crystal structure control, in the thermal annealing process, β-MoO_3 structure, a mixed structure of α-MoO_3 and β-MoO_3 structures, and α-MoO_3 structure can be produced by controlling the annealing temperature. In the FLA process, single-phase β-MoO_3 and α-MoO_3 structures can be

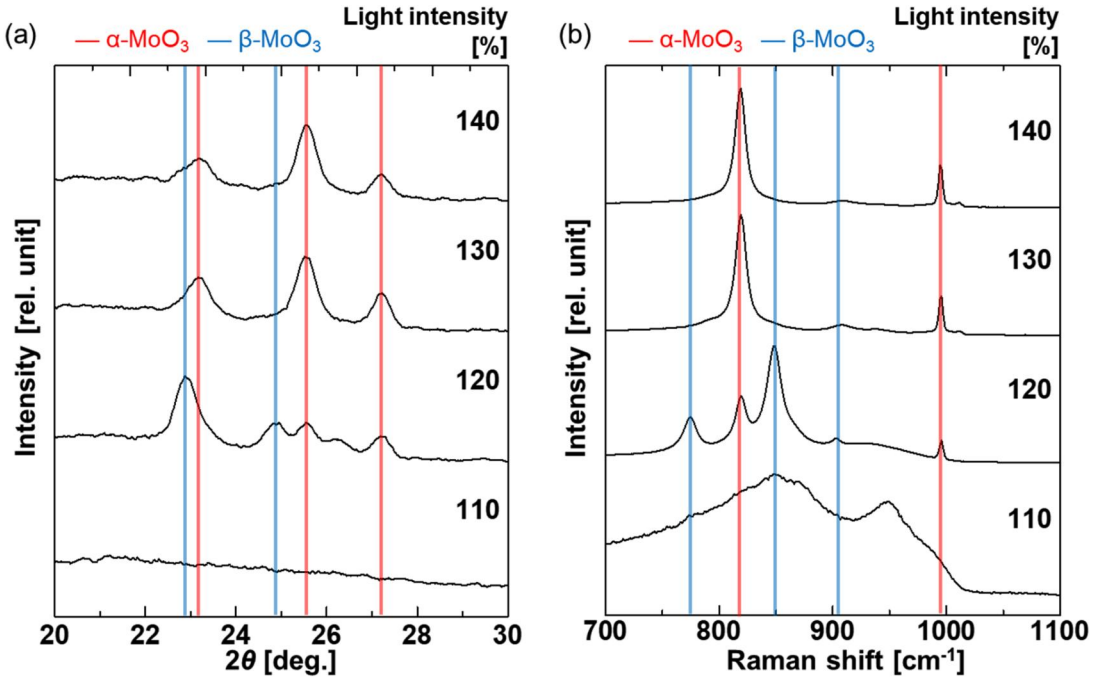

FIG. 6. XRD pattern and Raman spectra of the post-flashlamp annealed a-MoO_3 with cooling by liquid nitrogen. The red lines show the peaks corresponding to α-MoO_3 and the blue lines show the peaks corresponding to β-MoO_3. (a) XRD pattern (2θ scan), (b) Raman spectra.

produced by controlling the irradiation power. In conclusion, we have demonstrated that the crystal structures of MoO_3 can be controlled using post-treatment processes such as thermal annealing and flashlamp annealing.

See the supplementary material for additional characterization data, including full-range XRD patterns and Raman spectra for both post-thermal and post-flashlamp annealing processes as well as cross-sectional TEM images and electron diffraction patterns that support the crystalline phase identifications, along with detailed optical absorption spectra of the MoO_3 films and energy diagram illustrating the activation energy of crystallization and structural transitions.

This study was supported by JST, PRESTO, under Grant No. JPMJPR19I4, Japan, and JSPS KAKENHI Grant No. JP23K26055.

AUTHOR DECLARATIONS

Conflict of Interest

The authors have no conflicts to disclose.

Author Contributions

Makoto Kashiwagi: Conceptualization (equal); Data curation (equal); Formal analysis (equal); Funding acquisition (equal); Investigation (equal); Methodology (equal); Project administration (equal); Resources (equal); Supervision (equal); Validation (equal); Visualization (equal); Writing – original draft (equal); Writing – review & editing (equal). **Shota Chomei:** Data curation (equal); Formal analysis (equal); Investigation (lead); Methodology (equal); Validation (equal); Visualization (equal). **Takehiko Yokomori:** Investigation (supporting); Methodology (equal); Writing – review & editing (supporting). **Yuki Oguchi:** Investigation (supporting); Visualization (equal). **Yuzo Shigesato:** Conceptualization (lead); Formal analysis (equal); Funding acquisition (equal); Investigation (supporting); Methodology (lead); Project administration (lead); Resources (equal); Supervision (lead); Validation (equal); Visualization (equal); Writing – review & editing (equal).

DATA AVAILABILITY

The data that support the findings of this study are available from the corresponding author upon reasonable request.

REFERENCES

[1]C. G. Granqvist, S. Green, G. A. Niklasson, N. R. Mlyuka, S. von Kraemer, and P. Georén, Thin Solid Films **518**, 3046–3053 (2010).
[2]C. M. Lampert, Mater. Today **7**, 28–35 (2004).
[3]C. G. Granqvist, Sol. Energy Mater. Sol. Cells **60**, 201–262 (2000).
[4]Y. Shigesato, Jpn. J. Appl. Phys., Part 1 **30**, 1457 (1991).
[5]S. K. Deb, Sol. Energy Mater. Sol. Cells **92**, 245–258 (2008).
[6]J. L. He and M. C. Chiu, Surf. Coat. Technol. **127**, 43–51 (2000).
[7]X. Sun, Z. Liu, and H. Cao, Thin Solid Films **519**, 3032–3036 (2011).
[8]N. Oka, M. Watanabe, K. Sugie, Y. Iwabuchi, H. Kotsubo, and Y. Shigesato, Thin Solid Films **532**, 1–6 (2013).
[9]K. Nakagawa, N. Miura, S. Matsumoto, R. Nakano, and H. Matsumoto, Jpn. J. Appl. Phys., Part 1 **47**, 7230 (2008).
[10]T. Nanba, M. Ishikawa, Y. Sakai, and Y. Miura, Thin Solid Films **445**, 175 (2003).

[11]O. F. Schirmer, V. Wittwer, G. Baur, and G. Brandt, J. Electrochem. Soc. **124**, 749–753 (1977).
[12]P. Gérard, A. Deneuville, G. Hollinger, and T. M. Duc, J. Appl. Phys. **48**, 4252–4255 (1977).
[13]M. F. Saenger, T. Höing, B. W. Robertson, R. B. Billa, T. Hofmann, E. Schubert, and M. Schubert, Phys. Rev. B **78**, 245205 (2008).
[14]C.-S. Hsu, C.-C. Chan, H.-T. Huang, C.-H. Peng, and W.-C. Hsu, Thin Solid Films **516**, 4839–4844 (2008).
[15]A. Guerfi, R. W. Paynter, and L. Ê. H. Dao, J. Electrochem. Soc. **142**, 3457 (1995).
[16]D. Dixit, B. Ramachandran, M. Chitra, K. V. Madhuri, and G. Mangamma, Appl. Surf. Sci. **553**, 149580 (2021).
[17]H. Ding, H. Lin, B. Sadigh, F. Zhou, V. Ozoliņš, and M. Asta, J. Phys. Chem. C **118**, 15565–15572 (2014).
[18]T. He and J. Yao, J. Photochem. Photobiol., C **4**, 125–143 (2003).
[19]B. Dasgupta, Y. Ren, L. M. Wong, L. Kong, E. S. Tok, W. K. Chim, and S. Y. Chiam, J. Phys. Chem. C **119**, 10592–10601 (2015).
[20]O. Turel, S. O. Hacioglu, S. Coskun, L. Toppare, and H. E. Unalan, J. Electrochem. Soc. **164**, E565 (2017).
[21]Z. Hussain, J. Opt. Soc. Am. A **35**, 817–829 (2018).
[22]Ø. S. Fjellvåg, A. Ruud, H. H. Sønsteby, O. Nilsen, and H. Fjellvåg, Cryst. Growth Des. **20**(6), 3861–3866 (2020).
[23]C. G. Granqvist, *Handbook of Inorganic Electrochromic Materials* (Elsevier, Amsterdam, 1995).
[24]H. Wirth, D. Panknin, W. Skorupa, and E. Niemann, Appl. Phys. Lett. **74**, 979–981 (1999).
[25]A. Heya, N. Matsuo, S. Hirano, Y. Nakamura, T. Yokomori, and M. Yoshioka, in *Extended Abstracts of the 2015 International Conference on Solid State Devices and Materials* (IEEE, 2015), pp. 316–317.
[26]L. Rebohle, S. Prucnal, and D. Reichel, *Flash Lamp Annealing* (Springer, Berlin, 2019).
[27]B. Pécz, L. Dobos, D. Panknin, W. Skorupa, C. Lioutas, and N. Vouroutzis, Appl. Surf. Sci. **242**, 185–191 (2005).